Journal of Alloys and Compounds 506 (2010) 749–756

Contents lists available at ScienceDirect

Journal of Alloys and Compounds

journal homepage: www.elsevier.com/locate/jallcom

Enhanced electrochemical characteristics of as-spun nanocrystalline and amorphous Mg_2Ni-type alloy electrodes

Yang-huan Zhang[a,b,*], Shi-hai Guo[a], Yan Qi[a], Xia Li[a,b], Zhi-hong Ma[a,c], Yin Zhang[b]

[a] Department of Functional Material Research, Central Iron and Steel Research Institute, Beijing 100081, China
[b] School of Material, Inner Mongolia University of Science and Technology, Baotou 014010, China
[c] Baotou Research Institute of Rare Earths, Baotou 014010, China

ARTICLE INFO

Article history:
Received 7 May 2010
Received in revised form 7 July 2010
Accepted 7 July 2010
Available online 15 July 2010

Keywords:
Mg_2Ni-type alloy
Melt spinning
Substituting Ni with Mn
Electrochemical hydrogen storage

ABSTRACT

The nanocrystalline and amorphous Mg_2Ni-type electrode alloys with nominal compositions of $Mg_2Ni_{1-x}Mn_x$ (x = 0, 0.1, 0.2, 0.3, 0.4) are synthesized by melt-spinning technique. The spun alloy ribbons with a continuous length, a thickness of about 30 μm and a width of about 25 mm are obtained. The structures of the as-spun alloy ribbons are characterized by XRD, SEM and TEM. The electrochemical characteristics as well as the electrochemical impedance spectrums (EIS) of the as-spun alloy electrodes are measured. The hydrogen diffusion coefficients (D) in the alloys were obtained by virtue of potential-step method. The results show that the as-spun (x = 0) alloy holds a typical nanocrystalline structure, whereas the as-spun (x = 0.4) alloy displays a nanocrystalline and amorphous structure, confirming that the substitution of Mn for Ni evidently intensifies the glass forming ability of the Mg_2Ni-type alloy. The substitution of Mn for Ni significantly improves the electrochemical hydrogen storage performances of the alloys, involving the discharge capacity and the electrochemical cycle stability. Furthermore, the high rate discharge ability (HRD), the electrochemical impedance spectrum (EIS) and the potential-step measurements all indicate that the electrochemical kinetics of the alloy electrodes first increases then decreases with rising the amount of Mn substitution.

1. Introduction

Some Mg_2Ni-type compounds, such as Mg_2Ni, Mg_2Co and Mg_2Fe, have been expecting to be used as hydrogen storage materials or negative electrode in Ni–MH batteries [1] because of the great abundance, the light weight of Mg, and high hydrogen capacity of the hydrides, e.g. 3.6 wt.% for Mg_2NiH_4, 4.5 wt.% for Mg_2CoH_5 and 5.4 wt.% for Mg_2FeH_6. However, these kinds of the hydrides suffer from high thermodynamic stability, resulting in sluggish hydriding/dehydriding kinetics. Therefore, a variety of attempts, mechanical alloying (MA) [2], GPa hydrogen pressure method [3], melt spinning [4,5], gravity casting [6], hydriding combustion synthesis [7], surface modification [8], alloying with other elements [9], adding catalysts [10], spark plasma sintering [11], etc., have been developed to enhance their hydriding/dehydriding kinetics and to reduce their thermodynamic stability.

It was found that some amorphous Mg-based alloys prepared by mechanical alloying can electrochemically absorb and desorb a much larger amount of hydrogen at room temperature than their polycrystalline counterparts [12]. The notable improvement in the properties of these electrode materials was ascribed to the disordered character of the amorphous structure, which provides numerous desirable sites for electrochemical hydrogen storage. High energy ball milling, undoubtedly, is a very powerful method for the fabrication of the nanocrystalline and amorphous Mg and Mg-based alloys. Particularly, it is quite appropriate to solubilize the particular elements into MgH_2 or Mg_2NiH_4 above the thermodynamic equilibrium limit, which may facilitate the destabilization of MgH_2 or Mg_2NiH_4 [13]. However, the milled Mg_2Ni-type alloy electrodes exhibit extremely poor electrochemical cycle stability on account of the evanishment of the metastable structures formed by ball milling during the multiple electrochemical charging and discharging cycles [14], which is an insurmountable bottleneck for their practical application.

Alternatively, the melt-spun treatment can prohibit the rapid degradation of the hydrogen absorbing and desorbing cyclic characteristics of Mg and Mg-based compounds [5]. Furthermore, melt-spinning technique is an impactful method to yield a nanocrystalline structure and has been regarded to be the most appropriate for the mass-production of the nanocrystalline and amorphous Mg–Ni-based alloys. It has also been testified that the alloys with nanocrystalline and amorphous structure produced by

* Corresponding author at: Department of Functional Material Research, Central Iron and Steel Research Institute, 76 Xueyuan Nan Road, Haidian District, Beijing 100081, China. Tel.: +86 010 62187570; fax: +86 010 62184609.
E-mail address: zyh59@yahoo.com.cn (Y.-h. Zhang).

0925-8388/$ – see front matter © 2010 Elsevier B.V. All rights reserved.
doi:10.1016/j.jallcom.2010.07.060

melt-spinning method possess excellent electrochemical hydrogen storage characteristics, similar to that of the alloys fabricated by the MA process. Tanaka et al. [4] prepared the $Mg_{85}Ni_{10}La_5$ hydrogen storage alloy with a nanostructure by melt spinning to obtain reversible absorption and desorption amount of about 5 wt.% hydrogen at temperatures as low as 200 °C in moderate time periods. Huang et al. [5,15] reported that the amorphous and nanocrystalline Mg-based $(Mg_{60}Ni_{25})_{90}Nd_{10}$ alloy prepared by melt-spinning technique displays the highest discharge capacity of 580 mAh/g.

The objective of present work is to synthesize the Mg–Ni-based ternary nanocrystalline and amorphous alloys by melt-spinning technology and to examine their structures and electrochemical hydrogen storage characteristics.

2. Experimental

The alloy ingots were prepared using a vacuum induction furnace in a helium atmosphere at a pressure of 0.04 MPa in order to prevent volatilization of Mg during being melted. A part of the as-cast alloys was re-melted and spun with a rotating copper roller. The spinning rate was approximately expressed by the linear velocity of the copper roller because it is too difficult to measure a real spinning rate, i.e. cooling rate of the sample during spinning. The spinning rates used in the experiment were 15, 20, 25 and 30 m/s, respectively. The nominal compositions of the experimental alloys were $Mg_2Ni_{1-x}Mn_x$ (x = 0, 0.1, 0.2, 0.3, 0.4). For convenience, the alloys were denoted with Mn content as Mn_0, $Mn_{0.1}$, $Mn_{0.2}$, $Mn_{0.3}$ and $Mn_{0.4}$, respectively.

A Philips QUANTA 400 scanning electron microscope (SEM) linked with an energy dispersive spectrometer (EDS) was used for morphological characterization and chemical analysis of the as-cast alloys.

The phase structures of the as-cast and spun alloys were determined by X-ray diffractometer (XRD) (D/max/2400). The diffraction, with the experimental parameters of 160 mA, 40 kV and 10°/min respectively, was performed with $CuK_{\alpha 1}$ radiation filtered by graphite. The effective crystal sizes were calculated from Scherrer's formula following Williamson–Hall procedure [16].

The thin film samples of the as-spun alloys were prepared by ion etching technology in order to observe their morphologies with high resolution transmission electron microscope (HRTEM) (JEM-2100F, operated at 200 kV), and also to determine the crystalline state of the samples with electron diffraction (ED). The average grain sizes of the as-spun alloys were measured using a linear intercept method on the HRTEM micrographs.

The as-cast alloy bulk and the as-spun ribbons were pulverized by mechanical milling for 2 h, obtaining the powder samples of about 20 μm. Such powder is mixed with carbonyl nickel powder in a weight ratio of 1:4, and then is cold pressed under a pressure of 35 MPa into a round electrode pellet of 10 mm in diameter and total mass of about 1 g. A tri-electrode open cell, consisting of a metal hydride electrode, a sintered $NiOOH/Ni(OH)_2$ counter electrode and a Hg/HgO reference electrode, was used for testing the electrochemical characteristics of the experimental alloy electrodes. A 6 M KOH solution was used as electrolyte. The voltage between the negative electrode and the reference electrode was defined as the discharge voltage. In every cycle, the alloy electrode was first charged at a constant current density, and following the resting for 15 min, then it was discharged at the same current density to −0.500 V cut-off voltage. The environment temperature of the measurement was kept at 30 °C.

To determine the electrochemical kinetics of the alloy electrodes, electrochemical impedance spectra (EIS) were measured using an electrochemical workstation (PARSTAT2273). Prior to measuring the impedance, several electrochemical charging and discharging cycles were carried out in order to the alloy electrode be fully activated. The activated electrodes were fully charged and then rested for 2 h up to the stabilization of the open circuit potential. The EIS spectra of the alloy electrodes were obtained in the frequency range from 10 kHz to 5 mHz at 50% depth of discharge (DOD). For the potentiostatic discharge, the test electrodes in the fully charged state were discharged at 500 mV potential steps for 3500 s on the electrochemical workstation PARSTAT2273, using the CorrWare electrochemistry corrosion software.

3. Results and discussion

3.1. Microstructure characteristics

Depicted in Fig. 1 are the SEM images of the as-cast alloys. It is quite evident that the substitution of Mn for Ni visibly alters the morphologies of the major phase Mg_2Ni in the as-cast alloys from a typical dendrite structure to a featherlike one. The results obtained by SEM coupled with an energy dispersive spectrometry (EDS) indicate that the major phase of all the as-cast alloys retains invariably in the Mg_2Ni phase (denoted as A), but Mn substitution

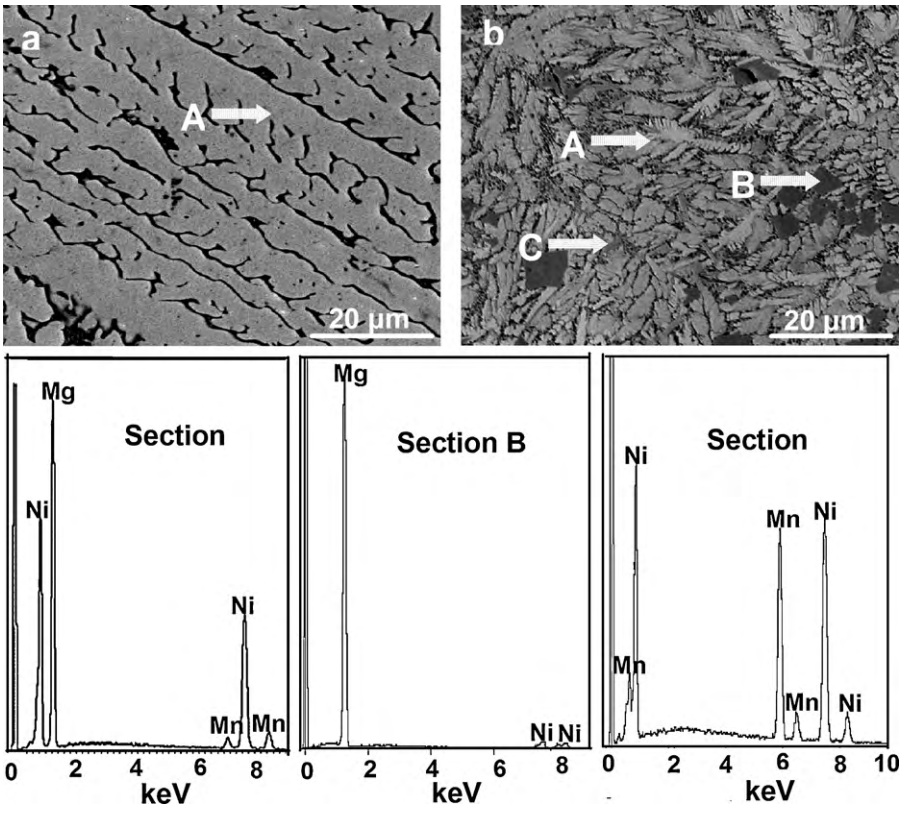

Fig. 1. SEM images of the as-cast alloys together with typical EDS spectra of sections A, B and C in (b): (a) Mn_0, (b) $Mn_{0.4}$.

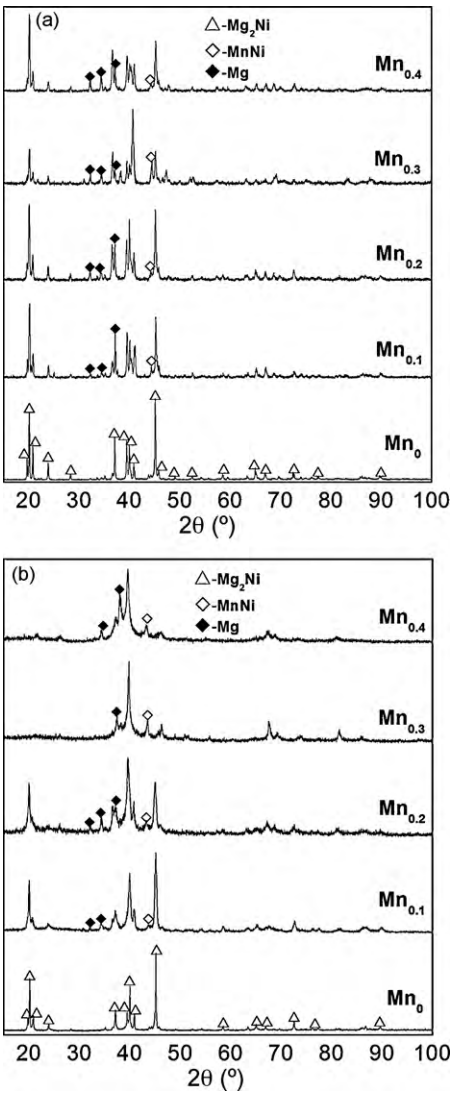

Fig. 2. XRD profiles of the as-cast and spun alloys: (a) as-cast, (b) as-spun (30 m/s).

leads to the formation of the secondary phases Mg (denoted as B) and MnNi (denoted as C).

The XRD profiles of the as-cast and spun alloys are presented in Fig. 2. The figure indicates that, instead of changing the major phase Mg_2Ni in the as-cast alloy, the substitution of Mn for Ni facilitates formation of secondary phases Mg and MnNi, and the amounts of which increase with rising Mn content except of the as-cast $Mn_{0.4}$ alloy. It is noteworthy that the as-cast $Mn_{0.4}$ alloy shows an evidently low amount of the MnNi phase, for which the heterogeneity of the as-cast alloy is mainly responsible since the componential segregation in the as-cast alloy is inevitable. It can be clearly seen in Fig. 2 that no amorphous phase is detected in the as-spun Mn_0 alloy, but the as-spun $Mn_{0.4}$ alloy shows the presence of an amorphous phase. Therefore, it can be concluded that the substitution of Mn for Ni intensifies the glass forming ability of the Mg_2Ni-type alloy. Two possibilities can be considered as the reasons for this result. Firstly, the additive third element to Mg–Ni or Mg–Cu alloys can significantly ease the glass formation [17,18]. Secondary, atomic radius of Mn is larger than Ni due to the fact that the glass forming ability of the alloy is closely associated with the difference of the atom radius of the alloy. The bigger the difference of the atom radius means the higher the glass forming ability of the alloy [19]. Listed in Table 1 are the lattice parameters, cell volume and full width at half maximum (FWHM) values of the main diffraction peaks of the as-cast and spun (30 m/s) alloys, which were calculated by Jade 6.0 software. It can be derived from Table 1 that the substitution of Mn for Ni causes not only a visible increase in the FWHM values of the main diffraction peaks of the alloys but also an evident enlargement in the lattice parameters and cell volume of the alloys, to be attributed to the larger atom radius of Mn than Ni. The melt-spinning inflicts a visibly increase in the FWHM values of the main diffraction peaks of the alloys which is doubtless attributed to the refined grains and the stored stress in the grains produced by melt spinning. Based on the FWHM values of the broad diffraction peak (2 0 3) in Fig. 2(b), the crystallite size $\langle D_{hkl}\rangle$ (nm) of the as-spun alloy is calculated using Scherrer's equation, to be in a range of 2–6 nm, basically consistent with results reported by Friedlmeier et al. [20]. It is noteworthy that for the comparison purposes, the $\langle D\rangle$ values have been calculated by using the similar peak having the Miller indices (2 0 3).

As the XRD analysis, a multiphase structure in the as-spun alloy is clearly detected by HRTEM. A grey block (denoted as A) and a white block with a regular polygon morphology (denoted as B) can been observed in Fig. 3, which are confirmed to be MnNi and Mg phases by EDS analysis.

The HRTEM micrographs and electron diffraction (ED) patterns of the as-spun (20 m/s) Mn_0 and $Mn_{0.4}$ alloys are illustrated in Fig. 4, displaying a nanocrystalline structure with an average crystal size of about 5 nm for Mn_0 alloy, and its ED pattern appears sharp multi-haloes, corresponding to a crystal structure. The as-spun $Mn_{0.4}$ alloy exhibits a distinct feature of the nanocrystalline embedded in the amorphous matrix, and its ED rings consist of broad and dull halo which confirms the emergence of an amorphous structure, suggesting that the substitution of Mn for Ni is beneficial for enhancing the glass forming ability of the alloy.

3.2. Electrochemical hydrogen storage performances

3.2.1. Electrochemical cycle stability

The electrochemical cycle stability of the alloy electrode is a decisive factor of the life of Ni–MH battery. The capacity retaining rate (S_n) was introduced to evaluate accurately the electrochemical cycle stability of the alloy, which is defined as $S_n = C_n/C_{max} \times 100\%$, where C_{max} is the maximum discharge capacity and C_n is the discharge capacity of the nth charge–discharge cycle, respectively. The Mn content dependence of the S_{20} ($n = 20$) values of the as-cast and

Table 1
Lattice parameters, cell volume and the FWHM values of the major diffraction peaks of the alloys.

Alloys	FWHM values				Lattice parameters and cell volume					
	2θ (20.02°)		2θ (45.14°)		a (nm)		c (nm)		V (nm^3)	
	As-cast	30 m/s	As-cast	30 m/s	As-cast	30 m/s	As-cast	30 m/s	As-cast	30 m/s
Mn_0	0.122	0.133	0.169	0.182	0.5210	0.5211	1.3244	1.3287	0.3113	0.3124
$Mn_{0.1}$	0.162	0.420	0.184	0.526	0.5212	0.5217	1.3252	1.3311	0.3117	0.3138
$Mn_{0.2}$	0.175	0.588	0.312	0.596	0.5215	0.5220	1.3297	1.3321	0.3131	0.3144
$Mn_{0.3}$	0.183	–	0.332	–	0.5217	–	1.3301	–	0.3135	–
$Mn_{0.4}$	0.189	–	0.371	–	0.5220	–	1.3306	–	0.3139	–

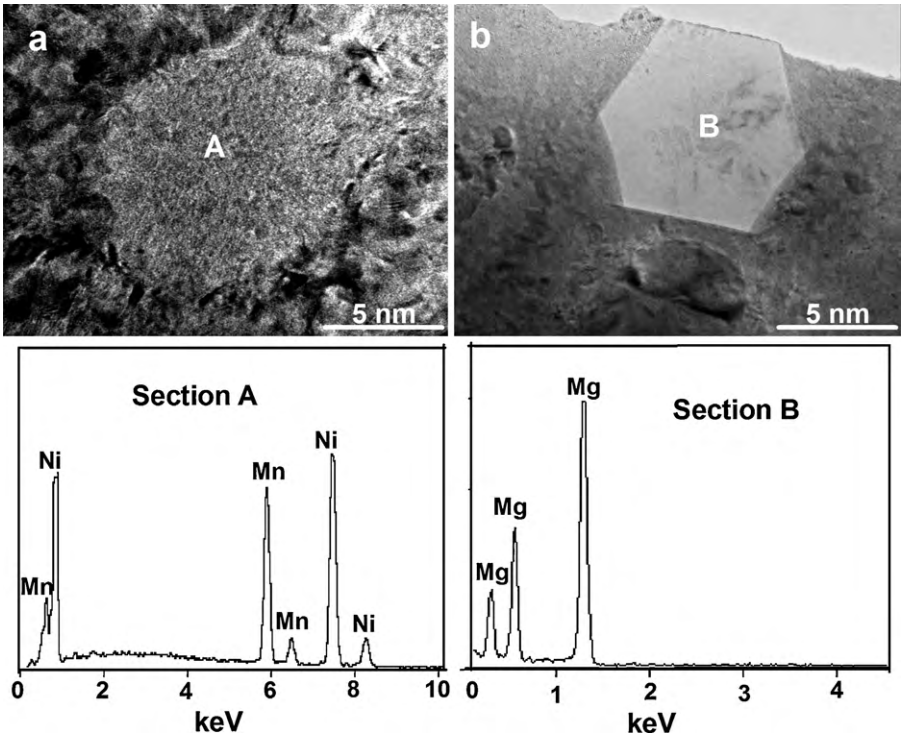

Fig. 3. HRTEM observation of Mg and MnNi phases in the as-spun (30 m/s) $Mn_{0.4}$ alloy together with typical EDS patterns of sections A and B in (a) and (b): (a) MnNi phase, (b) Mg phase.

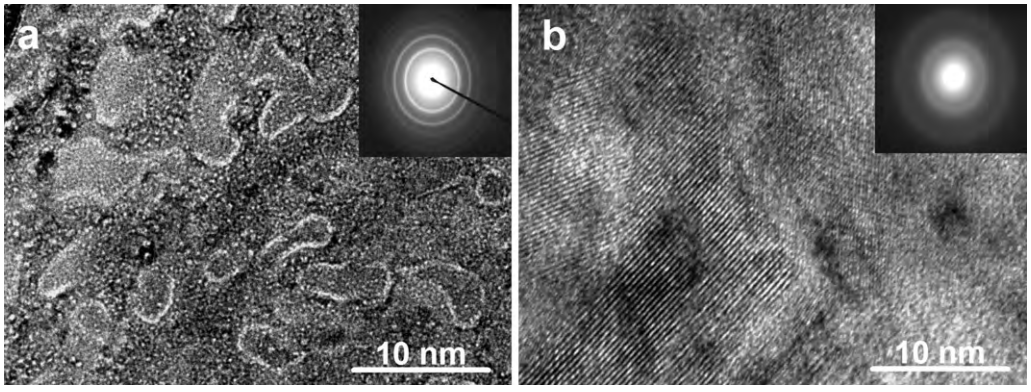

Fig. 4. HRTEM micrographs and ED patterns of the as-spun (20 m/s) alloys: (a) Mn_0 alloy, (b) $Mn_{0.4}$ alloy.

spun alloys is plotted in Fig. 5, indicating that the S_{20} values of the alloys always increase with rising the amount of Mn substitution. With the increase in Mn content x from 0 to 0.4, the S_{20} value increases from 33.5 to 36.7% for the as-cast alloy, and from 30.4 to 78.7% for the as-spun (30 m/s) alloy. Apparently, the positive impact of such substitution on the cycle stability is more pronounced for the as-spun alloy as compared to that for the as-cast one. It needs to be mentioned that, for a fixed Mn content, a higher spinning rate predicates a larger S_{20} value except the Mn_0 alloy.

In order to expressly see the process of the capacity degradation of the alloy electrode, the evolution of the S_n values of the as-cast and spun alloys with the cycle number is presented in Fig. 6, showing an evident tendency that the decay rate of the discharge capacity of the as-spun alloys conspicuously falls with rising Mn content, suggesting that the substitution of Mn for Ni enhances the cycle stability of the as-spun alloy. It was well known that the essential reason of which leads to the capacity degradation of the Mg-based alloy electrodes is the severe corrosion of Mg in the alkaline KOH solution. Especially, during the discharging

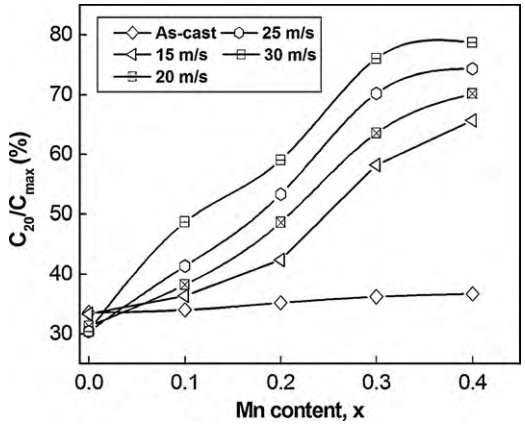

Fig. 5. Evolution of the capacity retaining rate (S_{20}) of the alloys with Mn content.

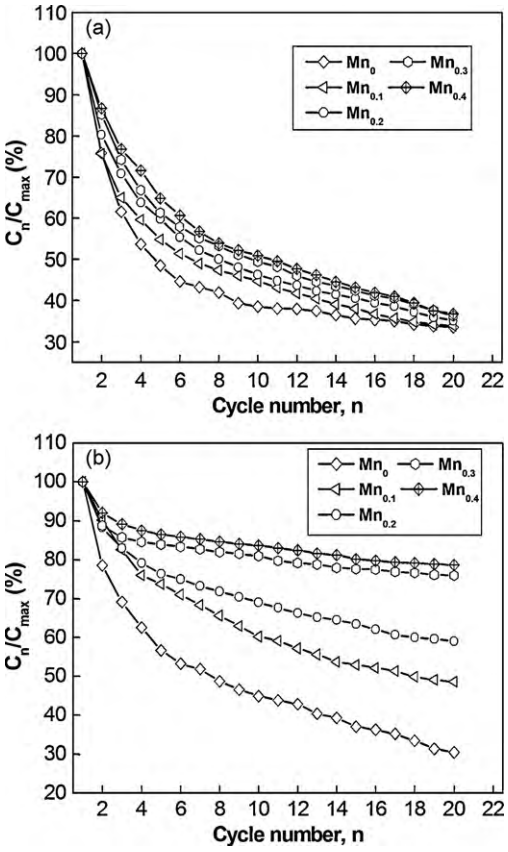

Fig. 6. Evolution of the capacity retaining rate of the alloys with cycle number: (a) as-cast, (b) 30 m/s.

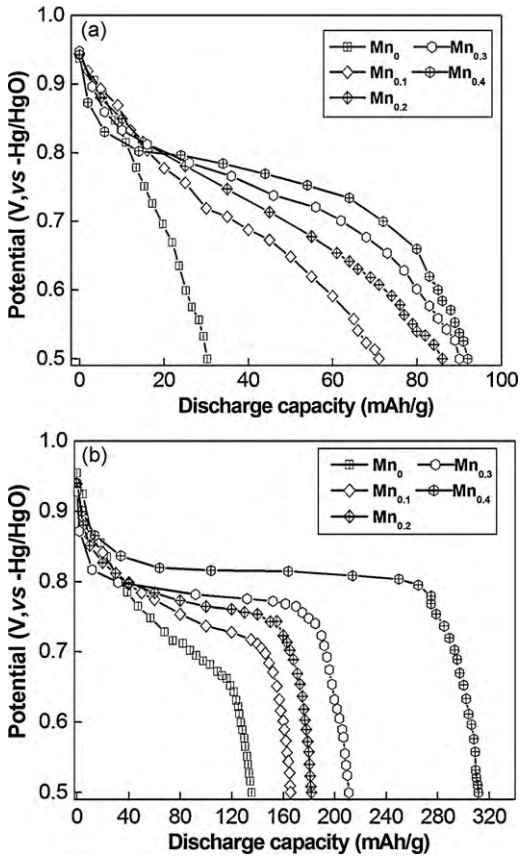

Fig. 7. Discharge curves of the as-cast and spun alloys: (a) as-cast, (b) as-spun (30 m/s).

process, the anodic polarization of the alloys facilitates the faster corrosion rate [21]. On the other hand, the metastable structures produced by melt spinning or ball milling tended to vanish during multiple charging/discharging cycles, which is an important factor for the capacity decay of the alloys. The positive impact of Mn substitution on the cycle stability of the alloy is ascribed to following reasons. One of which is that the enlarged cell volume by Mn substitution decreases the ratios of expansion/contraction of the alloys in process of the hydrogen absorption/desorption, meaning an increase in the anti-pulverization capability of the alloy. On the other hand, the enhanced glass forming ability by Mn substitution is extremely important because an amorphous phase improves not only anti-pulverization ability but also anti-corrosion and anti-oxidation abilities of the alloy electrode in a corrosive electrolyte [22]. Furthermore, the addition of a third element significantly stabilizes the nanostructure of the as-spun alloy [23], reflecting an enhancement in the cycle stability of the alloy.

3.2.2. Discharge potential and discharge capacity

Shown in Fig. 7 are the discharge curves of the as-cast and spun alloy electrodes at 20 mA/g at first charging/discharging cycle due to the fact that that all the alloys can be easily activated to reach the maximum capacity at first cycle. The figure evidently exhibits that the discharge potential plateaus in the discharge curves have the different width based on the oxidation of desorbed hydrogen from the hydride. The substitution of Mn for Ni notably modifies discharge potential characteristics of the as-spun (30 m/s) alloys, enhancing discharge potential and lengthening discharge plateau. It is quite evident that the substitution of Mn for Ni markedly increases the discharge capacity of the alloys. It is derived in Fig. 7 that the discharge capacity increases from 30.2 to 92.0 mAh/g for the as-cast alloy, and from 135.5 to 311.5 mAh/g for the as-spun

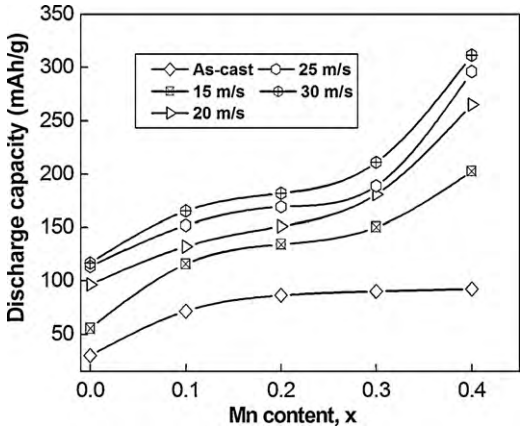

Fig. 8. Evolution of the maximum discharge capacity of the alloys with Mn content.

(30 m/s) alloy as the amount of Mn substitution rises from 0 to 0.4. It can be concluded by comparing Fig. 7(a) with (b) that the melt spinning not only markedly modifies the potential characteristic of the discharge curves but also remarkably heightens the discharge capacity of the alloys. Fig. 8 exhibits the relationship between the maximum discharge capacity of the alloy electrodes and the amount of Mn substitution. The figure indicates that the substitution of Mn for Ni visibly enhances the discharge capacity of the alloys. The observed result evidently reveals that Mn substitution engenders a more notable positive impact on the discharge capacity of the as-spun alloy than on that of as-cast one. It must be pointed out that, for a fixed Mn content, the discharge capacity of the alloy increases with rising spinning rate. The dis-

charge capacity of the alloy depends on multiple factors, involving its crystal structure, phase composition and structure, grain size, composition uniformity and surface state, etc. According to the result reported by Orimo and Fujii [24], the distribution of the maximum hydrogen concentrations in three nanometer-scale regions, i.e. grain region and grain-boundary region as well as amorphous region, have experimentally been determined to be 0.3 wt.% H in the grain region of Mg_2Ni, 4.0 wt.% H in the grain boundary and 2.2 wt.% H in the amorphous region. It reveals that the hydrides mainly exist in grain-boundary region and amorphous phase region. Several explanations may be offered as the reason why both the substitution of Mn for Ni and the melt spinning notably enhance the discharge capacity of the alloy. For the as-cast alloys, the substitution of Mn for Ni in Mg_2Ni compound lowers the thermal stability of the hydride which facilitates hydrogen desorption reaction [25,26]. The secondary phase MgNi probably works as a catalyst to activate the Mg_2Ni phase reversible absorbing/desorbing hydrogen in the alkaline electrolyte. For the as-spun alloys, the increased discharge capacity is ascribed to the intensified the glass forming ability of the alloys by Mn substitution. An appropriate ratio of amorphous and nanocrystalline exhibits an excellent discharge property of the Mg–Ni-based alloy [15]. The observed essential differences in the discharge capacity of the alloys caused by the melt spinning most probably have to be associated with the differences in their microstructures. The crystalline material, when melt spun, becomes at least partially disordered and its structure changes to nanocrystalline or amorphous. Consequently, the high densities of the crystal defects such as dislocations, stacking faults and grain boundaries are introduced. The large number of interfaces and grain boundaries available in the nanocrystalline materials accelerates the hydrogen absorbing/desorbing process on account of the fact that the easy pathways for hydrogen diffusion are provided. Additionally, as a result of the defects introducing distortion of crystal lattice, the stored sufficient energy as chemical disorder and the introduced defects (including both stacking faults as well as grain boundaries) will produce internal strain. It has been concluded by Niu and Northwood [27] that exchange current density and H-diffusion coefficient are directly proportional to the internal strain. Therefore, it is understandable that the introduction of defects and internal strain leads to an increase in the discharge capacity.

3.2.3. High rate dischargeability (HRD) and electrochemical kinetics

It is very important to restrain the decrease of the discharge capacity even at a high charge/discharge current density for the practical application of hydride electrode in Ni–MH battery. Generally, the electrochemical hydrogen storage kinetics of the alloy is characterized by its high rate dischargeability (HRD), being calculated according to the following formula: $HRD = C_{100,max}/C_{20,max} \times 100\%$, where $C_{100,max}$ and $C_{20,max}$ are the maximum discharge capacities of the alloy electrode charged–discharged at the current densities of 100 and 20 mA/g respectively. The HRD values of the alloy electrodes as a function of the Mn content are depicted in Fig. 9. It is clearly viewable in Fig. 9 that the HRD value of the as-cast alloy electrode always increases with growing Mn content whereas that of the as-spun alloy first mounts up then falls with the variation of Mn content. The optimum Mn content at which the alloy electrode obtains the largest HRD value is variational with the change of the spinning rate. As the amount of Mn substitution increases from 0 to 0.4, the HRD value rises from 30.7 to 53.2% for the as-cast alloy, and it mounts from 60.9% ($x = 0$) to 64.5% ($x = 0.1$) then declines to 43.2% ($x = 0.4$) for the as-spun (30 m/s) alloy. HRD value symbolizes a kinetic performance of hydrogen absorption/desorption of the alloy electrode, which principally depends on the charge transfer at the alloy–electrolyte interface and the hydrogen diffusion process from the interior of the bulk to the surface of alloy particle [28]. Two reasons are mainly responsible for the enhanced HRD values of the as-cast alloys by Mn substitution. On the one hand, the MnNi phase created by Mn substitution is beneficial to the diffusion of hydrogen atoms. On the other hand, Mn substitution accelerates the formation of a concentrated metallic Ni layer on the alloy surface of the alloy electrode which is highly beneficial to enhance the electrochemical catalytic property and to improve the reaction rate of hydrogen [29]. Furthermore, the presence of the optimum Mn content means that Mn substitution exerts beneficial and baneful impacts on the HRD value of the as-spun alloy. The benefaction of Mn substitution has been mentioned previously. And its detrimental impact on the HRD value of the alloy is attributed to the emergence of the amorphous phase created by Mn substitution. It is indubitable that the diffusion of hydrogen atoms is markedly easer in a crystal alloy than in an amorphous one due to the fact that the large number of interfaces and grain boundaries available can act as pathways for hydrogen diffusion [30]. Moreover, an amorphous phase can powerfully prohibits the pulverization of alloy during charging and discharging cycle [31] which may decrease the rate of charge transfer at the alloy–electrolyte interface due to available new surface of the alloy electrode becoming lower. It is these contrary factors that will result in an optimum Mn content as shown in Fig. 9.

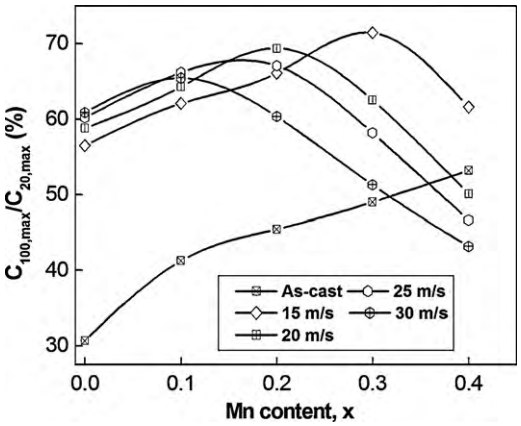

Fig. 9. Evolution of the high rate dischargeability (HRD) of the alloys with Mn content.

In order to determine the influence of Mn substitution on hydrogen diffusion ability in the alloy electrode, the hydrogen diffusion coefficients in selected the as-cast and spun (30 m/s) $Mg_2Ni_{1-x}Mn_x$ ($x = 0$–0.4) alloys were measured using potential-step method. Prior to the potential step, fresh electrode was fully charged and then rested for 2 h up to the stabilization of the open circuit potential. A potential step of +500 mV versus the stabilized open circuit potential of the fully charged electrode was applied and the decrease in discharge current was monitored as a function of time. Fig. 10 shows the semilogarithmic curves of the anodic current versus the working duration of the as-cast and spun (30 m/s) $Mg_2Ni_{1-x}Mn_x$ ($x = 0$–0.4) alloy electrodes, which can be divided into two time regions according to the analysis model proposed by Nishisa et al. [32] and Kuriyama et al. [33]. In the first time region, the current rapidly declined due to a consumption of hydrogen on the surface. In the other time region, however, the current slowly fell in a linear fashion in which the current was mainly controlled by the diffusion of hydrogen atoms with time. Thus, the diffusion coefficient D of the hydrogen atoms in the bulk of the alloy can be calculated through the slope of the linear region of the corresponding plots according to following formulae [34]:

$$\log \quad i = \log\left(\pm\frac{6FD}{da^2}(C_0 - C_s)\right) - \frac{\pi^2}{2.303}\frac{D}{a^2}t \qquad (1)$$

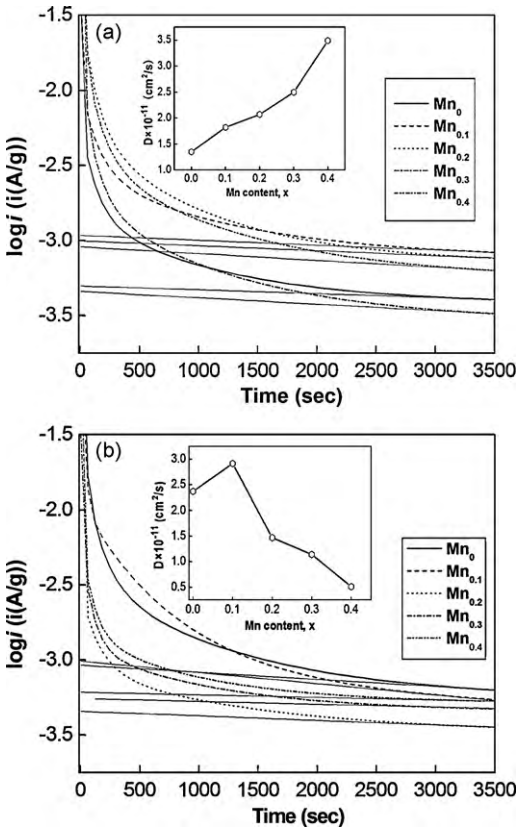

Fig. 10. Semilogarithmic curves of anodic current vs. time responses of the as-cast and spun alloy electrodes in fully charged state: (a) as-cast, (b) As-spun (30 m/s).

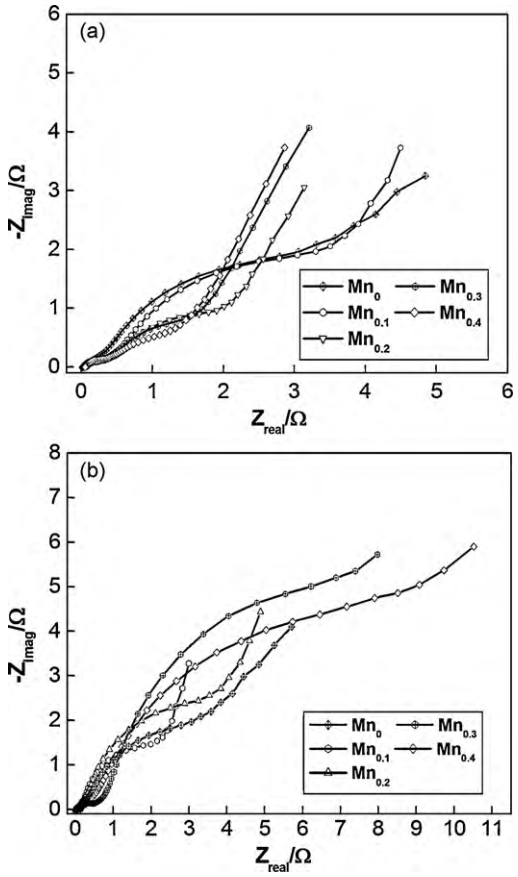

Fig. 11. Electrochemical impedance spectra (EIS) of the as-cast and spun alloy electrodes measured at the 50% depth of discharge (DOD): (a) as-cast, (b) as-spun (30 m/s).

$$D = -\frac{2.303a^2}{\pi^2}\frac{d\log\ i}{dt} \quad (2)$$

where i is the diffusion current density (A/g), D the hydrogen diffusion coefficient (cm^2/s), C_0 the initial hydrogen concentration in the bulk of the alloy (mol/cm^3), C_s the hydrogen concentration on the surface of the alloy particles (mol/cm^3), a the alloy particle radius (cm), d the density of the hydrogen storage alloy (g/cm^3), t the discharge time (s), respectively. The hydrogen diffusion coefficient D symbolizes the hydrogen diffusion rate in the bulk. The larger the diffusion coefficient, the faster is the diffusion of the hydrogen atoms in the alloy and the better is the electrochemical kinetics property of the alloy electrodes. The D values calculated by Eq. (2) are also illustrated in Fig. 10. It can be seen that the substitution of Mn for Ni inflicts a visible effect on H diffusion in the alloy. As the amount of Mn substitution grows from 0 to 0.4, the D value increases from 1.350×10^{-11} to 2.367×10^{-11} cm^2/s for the as-cast alloy, and it rises from 2.367×10^{-11} ($x = 0.0$) to 2.913×10^{-11} cm^2/s ($x = 0.1$) then falls to 0.51×10^{-11} cm^2/s ($x = 0.4$) for the as-spun (30 m/s) alloy. The benefaction of Mn substitution on the H diffusion coefficient in the as-cast alloy is attributed to the produced secondary phase MnNi and the enlarged cell volume by Mn substitution. An increased interface and grain boundary is highly helpful for enhancing H diffusion ability in the alloy electrode. The baneful action of Mn substitution on H diffusion in the as-spun alloy has been discussed anteriorly.

The electrochemical impedance spectra (EIS) of the as-cast and spun (30 m/s) alloy electrodes at 50% DOD are shown in Fig. 11. It is very evident that each EIS spectrum contains two semicircles followed by a straight line. Kuriyama et al. [33] founded a model in which the smaller semicircle in the high frequency region is attributed to the contact resistance between the alloy powder and the conductive material, and the larger semicircle in the low frequency region is attributed to the charge-transfer resistance on the alloy surface. The linear response at low frequencies is indicative of hydrogen diffusion in the bulk alloy. Hence, the electrode kinetics of the as-cast and spun alloys is dominated by a mixed rate-determining process. It can be seen in Fig. 11(a) that the radius of the large semicircle of the as-cast alloys in the low frequency continually shrinks with the increase in the amount of Mn substitution. This indicates that the charge-transfer resistance of the alloy electrode decreases with rising Mn content. The secondary phase MnNi in the alloy could play an important role to improve the electrocatalytic activity due to the fact that high active Raney Ni was probably generated at the electrode surface during the charging and discharging processes after the dissolution of Mn in a concentrated alkaline solution, leading to a reduction of the electrochemical reaction resistance. Fig. 11(b) shows that the radius of the large semicircle in the low frequency for the as-spun (30 m/s) alloy decreases first as Mn content rises from $x = 0$ to 0.1 and then enlarges as Mn content reaches $x = 0.2$. Apparently, the substitution of Mn for Ni inflicts the different impacts on the electrochemical kinetics of the as-cast and spun alloy electrodes, for which the change of the structure in the as-spun alloy caused by Mn substitution is mainly responsible. The crystalline materials, as quenched, become at least partially disordered, and at same time, various defects such as dislocations, stacking faults and grain boundaries are introduced. Thus, a large amount of internal energy would be stored and lead to non-stabilization of the lattice, yielding the fine grain sizes. The internal strain introduced by the defects accelerates hydrogen diffusion process since the exchange current density, diffusion coefficient are directly proportional to the internal strain. The large number of interfaces and grain boundaries available in the nanocrystalline

materials provide easy pathways for hydrogen diffusion [30]. Based on the above-mentioned results, it can be concluded that a suitable microstructure is one of the keys to obtain an optimized hydrogen storage kinetic property.

4. Conclusions

The investigation on the structures of the as-cast and spun $Mg_2Ni_{1-x}Mn_x$ (x = 0, 0.1, 0.2, 0.3, 0.4) alloys shows that no amorphous phase is detected in the as-spun Mn_0 alloy, but the as-spun $Mn_{0.4}$ alloys presents a feature of the nanocrystalline embedded in the amorphous matrix, confirming that the substitution of Mn for Ni facilitates the glass formation in the Mg_2Ni-type alloy. The substitution of Mn for Ni evidently improves the electrochemical hydrogen storage performances of the alloy, enhancing the discharge capacity and the electrochemical cycle stability, which is mainly attributed to the enlarged cell volume and the intensified glass forming ability by Mn substitution. Furthermore, the high rate dischargeability (HRD) of the as-cast alloy electrodes always increases with rising amount of Mn substitution, whereas for the as-spun alloy electrodes, it first increases then decrease with the incremental variation of Mn content. The results obtained from EIS and potential-step measurements agree well with the change of HRD value.

Acknowledgements

This work is supported by Hi-Tech Research and Development Program of China (2007AA03Z227), National Natural Science Foundations of China (50871050 and 50961001), Natural Science Foundation of Inner Mongolia, China (200711020703) and Higher Education Science Research Project of Inner Mongolia, China (NJzy08071).

References

[1] A. Ebrahimi Purkani, S.F. Kashani Bozorg, J. Alloys Compd. 456 (2008) 211–215.
[2] S.N. Kwon, S.H. Baek, D.R. Mumm, S.H. Hong, M.Y. Song, Int. J. Hydrogen Energy 33 (2008) 4586–4592.
[3] D. Kyoi, T. Sakai, N. Kitamura, A. Ueda, S. Tanase, J. Alloys Compd. 463 (2008) 306–310.
[4] K. Tanaka, T. Miwa, K. Sasaki, K. Kuroda, J. Alloys Compd. 478 (2009) 308–316.
[5] L.J. Huang, J.G. Tang, Y. Wang, J.X. Liu, D.C. Wu, J. Alloys Compd. 485 (2009) 186–191.
[6] M.Y. Song, C.D. Yim, J.S. Bae, D.R. Mummd, S.H. Hong, J. Alloys Compd. 463 (2008) 143–147.
[7] X.F. Liu, Y.F. Zhu, L.Q. Li, J. Alloys Compd. 455 (2008) 197–202.
[8] R. Janot, X. Darok, A. Rougier, L. Aymard, G.A. Nazri, J.M. Tarascon, J. Alloys Compd. 404–406 (2005) 293–296.
[9] C.X. Shang, M. Bououdina, Y. Song, Z.X. Guo, Int. J. Hydrogen Energy 29 (2004) 73–80.
[10] L. Xie, Y. Liu, X.Z. Zhang, J.L. Qu, Y.T. Wang, X.G. Li, J. Alloys Compd. 482 (2009) 388–392.
[11] J. Liu, X.P. Song, P. Pei, G.L. Chen, J. Alloys Compd. 486 (2009) 338–342.
[12] S. Mokbli, M. Abdellaoui, H. Zarrouk, M. Latroche, A. Percheron Guégan, J. Alloys Compd. 460 (2008) 432–439.
[13] G.Y. Liang, J. Alloys Compd. 370 (2004) 123–128.
[14] M.Y. Song, S.N. Kwon, J.S. Bae, S.H. Hong, Int. J. Hydrogen Energy 33 (2008) 1711–1718.
[15] L.J. Huang, G.Y. Liang, Z.B. Sun, D.C. Wu, J. Power Sources 160 (2006) 684–687.
[16] G.K. Williamson, W.H. Hall, Acta Metall. 1 (1953) 22–31.
[17] S.I. Yamaura, H.Y. Kim, H. Kimura, A. Inoue, Y. Arata, J. Alloys Compd. 339 (2002) 230–235.
[18] A. Inoue, T. Masumoto, Mater. Sci. Eng. A 173 (1993) 1–8.
[19] H.S. Chen, Acta Mater. 22 (1974) 1505–1511.
[20] G. Friedlmeier, M. Arakawa, T. Hiraia, E. Akiba, J. Alloys Compd. 292 (1999) 107–117.
[21] M.V. Simičić, M. Zdujić, R. Dimitrijević, Lj. Nikolić-Bujanović, N.H. Popović, J. Power Sources 158 (2006) 730–734.
[22] Y.H. Zhang, B.W. Li, H.P. Ren, Z.G. Pang, S.H. Guo, X.L. Wang, J. Alloys Compd. 477 (2009) 759–763.
[23] T. Spassov, U. Köster, J. Alloys Compd. 279 (1998) 279–286.
[24] S. Orimo, H. Fujii, Appl. Phys. A 72 (2001) 167–186.
[25] J.H. Woo, K.S. Lee, J. Electrochem. Soc. 146 (1999) 819–823.
[26] Y. Takahashi, H. Yukawa, M. Morinaga, J. Alloys Compd. 242 (1996) 98–107.
[27] H. Niu, D.O. Northwood, Int. J. Hydrogen Energy 27 (2002) 69–77.
[28] C. Iwakura, M. Matsuoka, K. Asai, T. Kohno, J. Power Sources 38 (1992) 335–343.
[29] A. Gasiorowski, W. Iwasieczko, D. Skoryna, H. Drulis, M. Jurczyk, J. Alloys Compd. 364 (2004) 283–288.
[30] Y. Wu, W. Hana, S.X. Zhou, M.V. Lototsky, J.K. Solberg, V.A. Yartys, J. Alloys Compd. 466 (2008) 176–181.
[31] Y.H. Zhang, H.P. Ren, S.H. Guo, Z.G. Pang, Y. Qi, X.L. Wang, J. Alloys Compd. 480 (2009) 750–755.
[32] T. Nishisa, H. Ura, I. Uchida, J. Electrochem. Soc. 144 (1997) 1273–1277.
[33] N. Kuriyama, T. Sakai, H. Miyamura, I. Uehara, H. Ishikawa, T. Iwasaki, J. Alloys Compd. 202 (1993) 183–197.
[34] G. Zhong, B.N. Popov, R.E. White, J. Electrochem. Soc. 142 (1995) 2695–2698.